Supporting information for

Assessing the Phosphate Distribution in Bioactive Phosphosilicate Glasses by ^{31}P Solid-State NMR and MD Simulations

Baltzar Stevensson, Renny Mathew and Mattias Edén*

Physical Chemistry Division, Department of Materials and Environmental Chemistry,

Arrhenius Laboratory, Stockholm University, SE-106 91 Stockholm, Sweden

*Corresponding author. E-mail: *mattias.eden@mmk.su.se*

Contents

S1 Effective ^{31}P–^{31}P Dipolar Coupling Constants: Experimental Obstacles

Here we discuss the reasons behind the 15–20% higher ^{31}P–^{31}P effective dipolar coupling constants reported in the present work relative to those of Mathew *et al.*[S1] for the same three $BG_{2.6}(2.1)$ ["45S5"], $BG_{4.0}(2.5)$ and $BG_{6.0}(2.5)$ glass *compositions*. There are primarily two experimental obstacles that previously compromised the determination of $b_{\text{eff}}^{\text{exp}}$ values obtained *via* fitting of the experimental 2QF amplitudes $\{a_{2\text{QF}}(\tau_{\text{exc}})\}$, both contributing towards underestimated coupling constants:

(**1**) NMR signal-damping stemming from ^{31}P relaxation during ^{31}P–^{31}P dipolar recoupling, whose impact is increased in the presence of paramagnetic species in the structure. The latter were introduced deliberately by doping each glass by 0.1 wt% Fe_2O_3 for the purpose of increasing the ^{31}P T_1-relaxation and thereby reducing the experimental time required to obtain quantitative NMR spectra. The *doped* glass samples of ref. S1 are henceforth referred to as "*dBG*". They allowed for complete equilibration within 40 s, whereas the "*undoped*" samples—here denoted "*BG*"—would require 12-30 minutes for equilibration between each NMR signal transient in the signal averaging procedure; see comment (*iv*) below. Unfortunately, the presence of Fe^{3+} ions also accelerated the relaxation of 2QC obtained from the dBG samples sufficiently much to compromise the $b_{\text{eff}}^{\text{exp}}$ estimates.

(**2**) Dipolar recoupling sequences may only recover a fraction—referred to as the dipolar *scaling factor* (κ)—of the ^{31}P–^{31}P dipolar interaction. For short τ_{exc}-values the 2QF signal buildup obeys[S1]

$$a_{2\text{QF}}(\tau_{\text{exc}}) \approx \frac{6}{5}(\kappa b_{\text{eff}}^{\text{exp}}\tau_{\text{exc}})^2, \tag{S1}$$

with κ=0.1743 for the $R20_2^9$ pulse scheme of Marin-Montesinos *et al.*[S2] under *ideal* experimental conditions. Unfortunately, *inhomogeneity* of the radio-frequency (rf) field across the powdered sample during dipolar recoupling may reduce the experimental 2QF NMR amplitude, as well as perturbing the scaling factor, altogether leading to an underestimation of the $b_{\text{eff}}^{\text{exp}}$-value extracted by fitting the experimental data to eq. (S1). Rf inhomogeneity may be reduced by restricting the sample volume in the rotor, however, at the expense of a significantly reduced NMR signal sensitivity that must be compensated for by a more extensive signal averaging and an accompanying increased experimental time. While all our previous NMR experimentation[S1] employed *full* rotors, the result reported in the main article involved samples confined to the mid 30% of the total rotor volume; this concerned the experimentation on both the BG and dBG specimens.

While we expected each obstacle (**1**) and (**2**) only to perturb primarily the long-term 2QC generation, together they turned out to also affect the initial $a_{2\text{QF}}(\tau_{\text{exc}})$-values sufficiently much to inflict a 15–20% underestimation of the effective dipolar coupling constants. While such an accuracy is by no means poor for this type of experimentation, it was insufficient for our particular task, which requires assessing the phosphate distribution in glasses whose P contents are both low and relatively close: the P content increases from 1.8 at% in $BG_{2.6}(2.1)$ to 4.1 at% in $BG_{6.0}(2.5)$, whereas their respective $b_{\text{eff}}^{\text{exp}}$-values display a square-root dependence on the amount of P; see Fig. **3**(b).

It is possible to *partially* compensate for the detrimental effects from relaxation and rf inhomogeneity by recording a complementary data-set, used for correcting the experimental $\{a_{2\text{QF}}(\tau_{\text{exc}})\}$ values, as described in detail by Saalwächter *et al.*[S3,S4] This procedure was employed herein, but not in our previous work.[S1] Table S1 lists the best-fit $b_{\text{eff}}^{\text{exp}}$-values obtained from each *directly* measured $\{a_{2\text{QF}}(\tau_{\text{exc}})\}$ set, as well as from their corrected counterparts. The table includes both the results from Mathew *et al.*[S1] that employed doped glass specimens in full rotors ("dBG-13"), those obtained from the *same* glass powders restricted to 30% of the total rotor volume (dBG), as well as from *undoped* BGs with restricted rotor-filling (BG). Note that only the latter data is discussed in the main article.

The following is noteworthy:

(*i*) Table S1 presents each effective dipolar coupling constant extracted by fitting its underlying

2QF amplitude-set, when including up to the first, second, and third $a_{2QF}(\tau_{exc})$ data-points, respectively. Note that the estimated b_{eff}^{exp}-value generally reduces when the number of fitted data-points is increased, i.e., when τ_{exc} grows. This reflects the validity of the approximation of eq. (S1), meaning that unless the experimental data are restricted to the shortest τ_{exc}-values of the 2QC buildup curve, the best-fit coupling constant becomes systematically underestimated.

(*ii*) Comparison of the effective coupling constants obtained from the BG and dBG samples reveals that the Fe^{3+}-doping resulted in a lower b_{eff}^{exp}-estimate by ≈7–8%. Moreover, a roughly equal underestimation emerged from the impact of rf inhomogeneity, as follows by comparing the data stemming from the use of full (dBG-13) and restricted (dBG) rotors. Altogether, these errors contribute to the net discrepancies of ≈15–20% between each b_{eff}^{exp}-value extracted in our present and previous[S1] work.

(*iii*) Table S1 reveals very similar b_{eff}^{exp}-values derived from the "corrected"[S3,S4] and "uncorrected" experimental 2QF amplitudes for the case of experimentation with undoped/restricted rotors (i.e., for which both NMR relaxation and rf inhomogeneity are minimized), whereas the data-correction has overall larger bearings for the doped glass samples. The first observation is gratifying concerning the reliability of the new b_{eff}^{exp}-estimates discussed in the main article.

(*iv*) While providing accurate b_{eff}^{exp}-values, the combination of omission of paramagnetic doping and use of restricted sample volumes makes this experimentation extremely time-consuming; it may be beneficial to omit the 2QF stage and instead monitor the magnetization-dephasing during 2Q recoupling, as recently demonstrated in other contexts by Ren and Eckert.[S5] Unfortunately, the absence of small amounts of paramagnetic species introduces *another potential source of underestimated coupling constants: T_1-effects*. The very slow ^{31}P T_1-relaxation makes it virtually impossible to perform recoupling experimentation by starting from thermal equilibrium (∼12–30 minutes, depending on the sample). All our experimentation involved a full saturation followed by a relaxation delay (τ_{relax} = 40 s) prior to the 2QF stage. For the two P-richest *undoped* $BG_{4.0}(2.5)$, and $BG_{6.0}(2.5)$ samples, we verified that no significant difference (<1%) resulted in the b_{eff}^{exp}-estimates if using τ_{relax} = 120 s or τ_{relax} = 40 s. These tests involved full rotors and Saalwächter's correction procedure. However, while the results from the $BG_{4.0}(2.5)$ glass were independent on τ_{relax}, the coupling constants were *underestimated* by ≈5% for $BG_{2.6}(2.1)$ and $BG_{6.0}(2.5)$ if employing shorter relaxation delays of 8 s (relative to those obtained for 40 s). Note that no peak-shape differences were discernible between the MAS spectra recorded by single pulses and employing either τ_{relax}-value, thereby not hinting of any potential problems and let alone offering any guidance for the selection of relaxation delays for the recoupling experimentation.

In conclusion, there are no doubts that our b_{eff}-values reported for the $BG_{4.0}(2.5)$ and $BG_{6.0}(2.5)$ specimens are converged with respect to τ_{relax}, whereas that of $BG_{2.6}(2.1)$ could *potentially* be slightly underestimated. This cannot be verified for τ_{relax} > 40 s owing to the prohibitively long experimentation required; however, its identical responses of b_{eff}^{exp} as those of the $BG_{6.0}(2.5)$ glass between data obtained for τ_{relax} = 8 s and τ_{relax} = 40 s strongly suggests that the latter b_{eff}^{exp}-value has already converged with respect to τ_{relax}.

S2 BG/MBG Experimental Data *versus* Random/Clustered Phosphate Distribution Scenarios

Figure S1(a) illustrates the various experimental b_{eff}^{exp} data from the BG, dBG and dBG-13 specimens of each $BG_{2.6}(2.1)$, $BG_{4.0}(2.5)$ and $BG_{6.0}(2.5)$ glass composition, plotted together with the results from the R(360), R(380) and R(420) models of randomly distributed phosphate groups. The bracketing of the dBG-13 data between those obtained by the R(380) and R(420) random distributions [R(411) was used as "lower" limit in ref. S1] made us advocate a scenario of randomly distributed orthophosphate groups in Na–Ca–Si–P–O BGs.[S1] This conclusion holds well also for the NMR results from restricted sample-filling of the Fe^{3+}-doped specimens (dBG). However, while the corresponding new results from

the undoped BGs largely accord with randomly distributed PO_4^{3-} groups subject to a minimum P–P interatomic distance of 360 pm [i.e., R(360)], the experimental $b_{\rm eff}^{\rm exp}$-values are consistently higher than those of the model. Moreover, the analysis of the MD-derived distribution also point to a somewhat higher phosphate-ion aggregation than that inherent to a simple statistical distribution, although the latter remains a good approximate description of the "real" P atom distribution.

Figure S1(b) additionally displays effective ^{31}P–^{31}P dipolar coupling constants obtained from the polycrystalline HAp reference, as well as from two CaO–SiO_2–P_2O_5 mesoporous bioactive glasses (MBGs) prepared by an evaporation-induced self-assembly process in the absence of paramagnetic doping.[S6,S7] For reasonable consistency with the present glass notation, they are denoted $S85_{3.4}$ and $S58_{4.3}$, where the subscript specifies the P_2O_5 content, with 85 mol% and 58 mol% SiO_2 respectively; hence, the CaO content is low/high for $S85_{3.4}$/$S58_{4.3}$. The open symbols represent the $b_{\rm eff}^{\rm exp}$-values reported earlier by Mathew *et al.*,[S1] obtained directly by fitting the $a_{\rm 2QF}(\tau_{\rm exc})$ data, whereas the filled symbols resulted by multiplying those $b_{\rm eff}^{\rm exp}$-values with the factor 1.08 to compensate for the effects from rf inhomogeneity.

Our previous conclusion remain, i.e., the two $S58_{4.3}$ and $S85_{3.4}$ structures exhibit a significantly enhanced orthophosphate clustering relative to their melt-prepared BG counterparts of comparable P_2O_5 content.[S1] The pore-walls of the Ca-richer $S58_{4.3}$ MBG was attributed to manifest a distribution of orthophosphate cluster-sizes $N^{\rm C} \lesssim 6$.[S1] This structural model is corroborated by Fig. S1(b) that also plots the $b_{\rm eff}$-values from randomly distributed $N^{\rm C}$=5 clusters selected from the α-$Ca_3(PO_4)_2$ and β-$Ca_3(PO_4)_2$ structures, labeled as C5[αCa] and C5[βCa], respectively: note that they manifest the lowest/highest effective dipolar couplings out of the simple orthophosphate structures (see Fig. 3 and discussion thereof). Moreover, a (melt-prepared) BG structure featuring $N^{\rm C}$=5 at 2.6 mol% P_2O_5 is likely to comprise *larger cluster-sizes* ($N^{\rm C}$>5) when its P content is increased (as opposed to an increased *number* of $N^{\rm C}$=5 clusters). To account for such a scenario, the CN(αCa) and CN(βCa) curves—depicted by open symbols and dotted lines in Fig. S1(b)—represent the corresponding $b_{\rm eff}$-values associated with randomly distributed $N^{\rm C}$=8 and $N^{\rm C}$=12 clusters for BGs with 4.0 mol% and 6.0 mol% P_2O_5, respectively. These cluster sizes were predicted from the relative increase in P contents. The much higher $b_{\rm eff}$-value of the $S85_{3.4}$ structure (only second to the macroscopic system of dipolar-coupled $^{31}PO_4$ groups in HAp) reflects pore-walls that exhibit a significant P clustering, estimated conservatively to involve clusters comprising 20–40 phosphate groups.[S1]

Table S1: Double-Quantum-Derived Effective ^{31}P–^{31}P Dipolar Coupling Constants[a]

	$-b_{\mathrm{eff}}^{\mathrm{exp}}/2\pi$ [Hz]		
	$BG_{2.6}(2.1)$	$BG_{4.0}(2.5)$	$BG_{6.0}(2.5)$
BG	228–**221**–223	281–**291**–285	347–**342**–335
	223–217–212	272–287–282	343–337–328
dBG	n.d.	262–267–263	337–317–315
	n.d.	259–260–255	329–305–303
dBG-13[S1]	n.d.	n.d.	n.d.
	200–189–189	**243**–236–224	**296**–284–269
HAp[b]	661–**646**–627		
	661–648–628		
	609–609–582[S1]		

[a]Effective dipolar coupling constant $b_{\mathrm{eff}}^{\mathrm{exp}}$ derived from the as-indicated glasses that were prepared in the presence (dBG) or absence (BG) of 0.1 wt% Fe_2O_3. The $b_{\mathrm{eff}}^{\mathrm{exp}}$-values are listed according to *a–b–c;* they were obtained by fitting the sets comprising up to one, two, and three points of the 2QF curves presented in Fig. 3, respectively. The *lower row* of numbers for each sample comprise the best-fit $b_{\mathrm{eff}}^{\mathrm{exp}}$-values from the directly measured experimental 2QF data, whereas the *upper row* lists the corresponding "*corrected*" constants *via* the procedure described by Saalwächter *et al.*[S3,S4] Bold-face numbers are the *selected* $b_{\mathrm{eff}}^{\mathrm{exp}}$-values, i.e., those discussed in the present paper (BG), or in our previous work (dBG-13).[S1]

[b]$b_{\mathrm{eff}}^{\mathrm{exp}}$-values extracted from a powder of polycrystalline HAp, *restricted* to the 30% center of the rotor, and obtained in the *presence* (*top* row) and *absence* (*mid* row) of 2QF data-correction. The bottom row of data are reproduced from Mathew *et al.*;[S1] they were obtained by employing a *full* rotor and doped samples for the 2QF experiments.

Table S2: Molecular Dynamics Simulation Parameters and Results

Sample label	N_{tot}[a]	N_{P}[a]	N_{Si}[a]	N_{sim}[a]	a/nm[b]	ρ_{exp}/gcm^{-3} [c]	Q^n_{P} populations[d] x^0_{P}	x^1_{P}	x^2_{P}	$\mathcal{R}^{\mathrm{P-P}}_{\mathrm{Si-P}}(450)$[e]	$\mathcal{R}^{\mathrm{P-P}}_{\mathrm{Si-P}}(600)$[e]
$BG_{2.6}(2.1)$	10017	184	1632	2	5.114	2.704	0.959(0.834)	0.041(0.166)	0.000(0.000)	1.20	1.41
$BG_{6.0}(2.1)$	6123	252	829	2	4.336	2.743	0.955(0.798)	0.045(0.200)	0.000(0.002)	1.45	1.38
$BG_{1.0}(2.5)$	12279	88	2416	4	5.473	2.685	0.899(0.690)	0.101(0.299)	0.000(0.011)	1.09	1.60
$BG_{2.0}(2.5)$	5768	80	1076	3	4.257	2.691	0.896(0.721)	0.104(0.267)	0.000(0.013)	1.36	1.34
$BG_{4.0}(2.5)$	6280	176	1044	4	4.379	2.693	0.931(0.622)	0.069(0.364)	0.000(0.014)	1.38	1.37
$BG_{6.0}(2.5)$	5644	232	828	2	4.223	2.707	0.902(0.690)	0.098(0.304)	0.000(0.006)	1.27	1.42
$BG_{2.6}(2.7)$	9999	180	1909	2	5.129	2.635	0.838(0.517)	0.162(0.475)	0.000(0.008)	1.22	1.48
$BG_{2.0}(2.9)$	6080	88	1272	3	4.347	2.624	0.795(0.417)	0.205(0.553)	0.000(0.030)	1.19	1.41
$BG_{3.0}(2.9)$	6081	126	1205	2	4.350	2.625	0.814(0.445)	0.186(0.528)	0.000(0.028)	1.17	1.59
$BG_{4.0}(2.9)$	6372	176	1192	4	4.414	2.639	0.805(0.442)	0.195(0.542)	0.000(0.016)	1.20	1.48
$BG_{6.0}(2.9)$	6000	240	996	2	4.320	2.661	0.821(0.460)	0.179(0.527)	0.000(0.012)	1.15	1.47

[a] N_{tot} represents the total number of atoms in the simulation, whereas N_{P} and N_{Si} correspond to those of P and Si, respectively, and N_{sim} is the number of independent glass models generated.

[b] Side length of the cubic box.

[c] Experimental density, reproduced from ref. S8.

[d] Fractional population x^n_{P} of Q^n_{P} groups, as obtained experimentally by ^{31}P MAS NMR, or by MD simulations (within parenthesis).[S8]

[e] The factor $\mathcal{R}^{\mathrm{P-P}}_{\mathrm{Si-P}}(r) = \overline{\mathrm{CN}}_{\mathrm{P-P}}/\overline{\mathrm{CN}}_{\mathrm{Si-P}}$, where $\overline{\mathrm{CN}}_{\alpha-\beta}$ represents the average coordination number of species α with respect to β over a radius r;[S9] the uncertainty of $\mathcal{R}^{\mathrm{P-P}}_{\mathrm{Si-P}}(r)$ is ± 0.15.

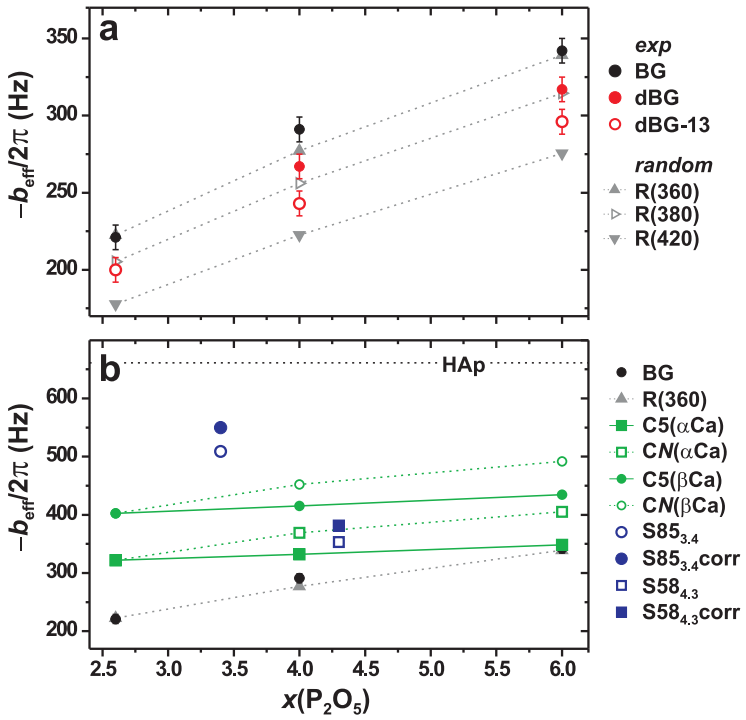

Fig. S1. (a) NMR-derived ^{31}P–^{31}P effective dipolar coupling constants from the as-indicated glass specimens of the $BG_{2.6}(2.1)$, $BG_{4.0}(2.5)$, and $BG_{6.0}(2.5)$ compositions (see section S1), shown together with b_{eff}-values calculated from randomly distributed P *atoms*; R(d_{min}), with $d_{\text{min}} = \{360, 380, 420\}$ pm. (b) Calculated b_{eff}-values for various phosphate *clustering* scenarios and experimental data from two MBG specimens. The latter were reproduced directly from Mathew *et al.*[S1] ($S85_{3.4}$; $S58_{4.3}$), as well as subjected to an approximate correction for rf inhomogeneity ($S85_{3.4}$corr; $S58_{4.3}$corr). The dotted line marks the experimentally determined effective dipolar coupling constant for HAp. Other details are provided in section S2.

References

(S1) Mathew, R.; Turdean-Ionescu, C.; Stevensson, B.; Izquierdo-Barba, I.; García, A.; Arcos, D.; Vallet-Regí, M.; Edén, M. Direct Probing of the Phosphate-Ion Distribution in Bioactive Silicate Glasses by Solid-State NMR: Evidence for Transitions between Random/Clustered Scenarios. *Chem. Mater.* **2013**, *25*, 1877–1885.

(S2) Marin-Montesinos, I.; Brouwer, D. H.; Antonioli, G.; Lai, W. C.; Brinkmann, A.; Levitt, M. H. Heteronuclear Decoupling Interference During Symmetry-Based Homonuclear Recoupling in Solid-State NMR. *J. Magn. Reson.* **2005**, *177*, 307–317.

(S3) Saalwächter, K.; Ziegler, P.; Spyckerelle, O.; Haider, B.; Sommer, J.-U. ^{1}H Multiple-Quantum Nuclear Magnetic Resonance Investigations of Molecular Order Distributions in Poly(Dimethylsiloxane) Networks: Evidence for a Linear Mixing Law in Bimodal Systems. *J. Chem. Phys.* **2003**, *119*, 3468–3482.

(S4) Saalwächter, K.; Lange, F.; Matyjaszewski, K.; Huang, C.-F.; Graf, R. BaBa-xy16: Robust and Broadband Homonuclear DQ Recoupling for Applications in Rigid and Soft Solids up to the Highest MAS Frequencies. *J. Magn. Reson.* **2011**, *212*, 204–215.

(S5) Ren, J.; Eckert, H. DQ-DRENAR: A New NMR Technique to Measure Site-Resolved Magnetic Dipole-Dipole Interactions in Multispin-1/2 Systems: Theory and Validation on Crystalline Phosphates. *J. Chem. Phys.* **2013**, *138*, 164201.

(S6) Mathew, R.; Gunawidjaja, P. N.; Izquierdo-Barba, I.; Jansson, K.; García, A.; Arcos, D.; Vallet-Regí, M.; Edén, M. Solid-State ^{31}P and ^{1}H NMR Investigations of Amorphous and Crystalline Calcium Phosphates Grown Biomimetically from a Mesoporous Bioactive Glass. *J. Phys. Chem. C* **2011**, *115*, 20572–20582.

(S7) Gunawidjaja, P. N.; Mathew, R.; Lo, A. Y. H.; Izquierdo-Barba, I.; García, A.; Arcos, D.; Vallet-Regí, M.; Edén, M. Local Structures of Mesoporous Bioactive Glasses and Their Surface Alterations in Vitro: Inferences from Solid State Nuclear Magnetic Resonance. *Phil. Trans. R. Soc. A* **2012**, *370*, 1376–1399.

(S8) Mathew, R.; Stevensson, B.; Tilocca, A.; Edén, M. Toward a Rational Design of Bioactive Glasses with Optimal Structural Features: Composition-Structure Correlations Unveiled by Solid-State NMR and MD Simulations. *J. Phys. Chem. B* **2014**, *118*, 833–844.

(S9) Tilocca, A. Cooling Rate and Size Effects on the Medium-Range Structure of Multicomponent Oxide Glasses Simulated by Molecular Dynamics. *J. Chem. Phys.* **2013**, *139*, 114501.